12th SPIE International Symposium on Smart Structures and Smart Materials

Ferritin-Templated Quantum-Dots for Quantum Logic Gates

Sang H. Choi[1], Jae-Woo Kim[2], Sang-Hyon Chu[3], Yeonjoon Park[2], Glen C. King[1], Peter T. Lillehei[1], Seon-Jeong Kim[4], and James R. Elliott[1]

[1] NASA Langley Research Center, Hampton, VA 23681
[2] Science & Technology Corp., Hampton, VA 23666
[3] National Institute of Aerospace, Hampton, VA 23666
[4] Hanyang University, Seoul, Korea

Abstract

Quantum logic gates (QLGs) or other logic systems are based on quantum-dots (QD) with a stringent requirement of size uniformity. The QD are widely known building units for QLGs. The size control of QD is a critical issue in quantum-dot fabrication. The work presented here offers a new method to develop quantum-dots using a bio-template, called ferritin, that ensures QD production in uniform size of nano-scale proportion. This technology is essential for NASA, DoD, and industrial nanotechnology applications such as: ultra-high density data storage, quantum electronic devices, biomedical nanorobots, molecular tagging, terahertz radiation sources, nanoelectromechanical systems (NEMS), etc. The bio-template for uniform yield of QD is based on a ferritin protein that allows reconstitution of core material through the reduction and chelation processes. By either the magnetic or electrical property of reconstituted core materials, the QD can be used for logic gates which are fundamental building blocks for quantum computing. However, QLGs are in an incubation stage and still have many potential obstacles that need to be addressed, such as an error collection, a decoherence, and a hardware architecture. One of the biggest challenges for developing QLG is the requirement of ordered and uniform size of QD for arrays on a substrate with nanometer precision. The other methods known so far, such as self-assembled QD grown in the Stranski-Krastanov mode, are usually randomly organized. The QD development by bio-template includes the electrochemical/chemical reconsitution of ferritins with different core materials, such as iron, cobalt, manganese, platinum, and nickel. The other bio-template method used in our laboratory is dendrimers, precisely defined chemical structures. With ferritin-templated QD, we fabricated the heptagon-shaped patterned array via direct nano manipulation of the ferritin molecules with a tip of atomic force microscope (AFM). We also designed various nanofabrication methods of QD arrays using a wide range manipulation techniques. The precise control of the ferritin-templated QD for a patterned arrangement are offered by various methods, such as a site-specific immobilization of thiolated ferritins through local oxidation using the AFM tip, ferritin arrays induced by gold nanoparticle manipulation, thiolated ferritin positioning by shaving method, etc. In the signal measurements, the current-voltage curve is obtained by measuring the current through the ferritin, between the tip and the substrate for potential sweeping or at constant potential. The measured resistance near zero bias was 1.8 teraohm for single holoferritin and 5.7 teraohm for single apoferritin, respectively.

General Description of Principles

The quantum dots are based on the ferritin protein, naturally existing iron storage proteins, consisting of a segmented protein shell with an outer diameter of 12 nm and an inner diameter of 8 nm, surrounded by 24 polypeptide subunits [1]. Basically, the magnetic and/or electrical properties of quantum dot-scale ferritins allow the formation of logic gates, which are fundamental building blocks for quantum computing [2-4]. The proposed tasks explored the quantum aspects of ferritins for a quantum dot cellular automata (QCA) logic simulator. The principles of the current research activities are based on the following:

Quantum Computing Simulator: Computing power has increased at an amazing rate over the last few decades by chip miniaturization. If the feature size of chip were to be decreased further to the scale of tens of nanometers, their operation would be seriously disrupted by the occurrence of quantum phenomena, such as electrons tunneling through the barriers between wires. On the contrary, quantum computers will work through quantum effects to sustain immense computing power. However, a few difficult obstacles such as decoherence still pre-

vent us from building a quantum computer that can rival today's classical digital computer. Quantum computer research appeared in 1980's has become more and more vigorous due to the discovery of quantum algorithms and the developments of nano-scale experimental techniques in recent years [5-7]. Any candidates for quantum computing should be assessed against quantum hardware checklist suggested by DiVincenzo [7]. The five criteria of 'DiVincenzo checklist' are as follows: (1) clearly identifiable qubits (quantum bit) and the ability to scale up in number (In a fabricated system of many particles/clusters, every molecular particle/cluster can act as an individual qubit, identifiable through its spatial location. There are two potential realizations of a qubit. Case I, the classical picture of the $|1\rangle$ state (the excited state) is the uniform precession of the magnetic moment of the particle about the direction of the effective field that is formed by the magnetic anisotropy of the particle and the external magnetic field. This excited state is separated from the ground state, $|0\rangle$. Case II, the qubit states correspond to the symmetric, $|0\rangle$, and antisymmetric, $|1\rangle$, combinations of the twofold degenerate ground state $S_Z = S$. The energy splitting between the qubit states depends on the spin tunneling frequency and can be tuned using an external magnetic field perpendicular to the easy axis of the molecular cluster.); (2) state preparation – the ability to prepare the thermal ground state of the whole system (State preparation must be realized at a temperature significantly lower than the energy gap, Δ, between the states $|0\rangle$ and $|1\rangle$. The typical gap for Case I is of the order of a few Kelvin, while in Case II the gap may be controlled by applying an external magnetic field perpendicular to the anisotropy axis of the molecular cluster.); (3) low decoherence – error correction technique are needed; (4) quantum gates – the ability to realize a universal set of gates through control of the system Hamiltonian; and (5) capability of measurement on the qubits to obtain the result of the computation. Theoretically, the magnetic nanoparticle system proposed is a good candidate for quantum computing [8]. In a quantum computer, the state of each quantum nanoparticle is permitted to be any quantum-mechanical state of qubit. Computation of quantum computer proceeds by a sequence of two-qubit quantum gates [9], coherent interactions involving specific pairs of qubits, by analogy to the realization of ordinary digital computation as a sequence of Boolean logic gates. It is now understood that the time evolution of an arbitrary quantum state is more powerful computationally than the evolution of a digital logic state. The quantum computation can be illuminated as a coherent superposition of digital computations proceeding in parallel.

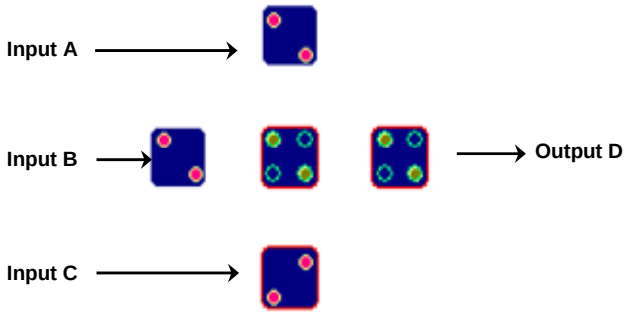

Figure 1. Proof-of-concept for protein-based quantum computing simulator: a quantum-dot cellular

Quantum Logic Gates-QCA Majority Gate: The distinctive feature of a quantum computer is its ability to store and process superpositions of states. The quantum computer hosts a register of qubits, which behave as quantum mechanical two-level systems and can be used to store arbitrary superposition states (0 and 1). The proof-of-concept simulator gate proposed here is a QCA majority gate as shown in Fig. 1. It is a 3-input, single output binary logic gate with the following truth table (Table I). The binary logic function AND is achieved by setting one of the inputs equal to 0 (e.g. $[(C \rightarrow 0) \rightarrow (A \wedge B)]$). The binary logic function OR is achieved by setting one of the inputs equal to 1 (e.g. $[(C \rightarrow 1) \rightarrow (A \vee B)]$). Therefore, the combination of the QCA majority gate and the QCA inverter constitute a universal set of gates for binary logic. Ohshima et al. fabricated the quantum logic gate with $In_{0.4}Ga_{0.6}As$ quantum dots using AFM lithography [10]. They prepared a quantum dot array where one qubit consists of a big quantum dot as the main dot and a few small quantum dots as the operation dots, the big and small dots of ~ 30 nm and ~ 20 nm in diameter, respectively, and the center-to-center distance between big and small dots of 40 nm as shown in Fig. 2. In this work, the inter-qubit coupling is controlled by pushing an electron into the main dots (weakly or not coupled) or neighboring operation dots (strongly coupled). In the stand-by state, the electron with spin up or down stays in the main dot. Applying a suitable π-pulse to any qubit, the electron will transfer to an operation dot. The quantum gate operation is implemented via swapping between the electron spins in operation dots belonging to neighboring qubits.

Why Ferritin?: Ferritin is an iron storage protein involved widely in biological mechanisms, containing up to ~ 4500 Fe^{3+} ions as ferrihydrite ($5Fe_2O_3 \cdot 9H_2O$) within their hollow, spherical protein interior [1]. The assem-

bled structure of ferritin is remarkably stable and robust, able to withstand biologically extremes of high temperature (up to 80 ^{o}C) and pH variations (2.0 ~ 10.0) [11]. The ferritin molecule has eight hydrophilic channels along the three-fold symmetry axes and six hydrophobic channels along the four-fold symmetry axes. The hydrophilic channels that penetrate the protein shell are considered to be the pathways of Fe^{2+}. Demetalated ferritin (apoferritin) can be loaded with inorganic mineral phases through hydrophilic or hydrophobic channels of protein shell, such as cobalt [11], manganese [12-14], nickel [15], cadmium sulfide [16], magnetite-maghemite (Fe_3O_4/γ-Fe_2O_3) [17,18], and trimethylamine-N-oxide (Me_3NO) [18]. The magnetic state of ferritins depends on core materials: ferrihydrite is known to be antiferromagnetic; maghemite is ferrimagnetic; Me_3NO is superparamagnetic. It is noted that this magnetic state is also sensitive to temperature and core size that can be controlled by metal loading values per ferritin. Natural horse spleen ferritin (HoSF) becomes antiferromagnetic at the Néel ordering temperature of T_N ~ 240 K [3]. However, the natural ferritins are in fact superparamagnetic (i.e. single domain Néel order is well established in each HoSF, but its direction fluctuates in time) below T_N [2]. Quantum tunneling of the magnetization in antiferromagnets is much stronger than in ferromagnets. Fabrication of magnetic core sizes with narrow distribution could enable resonance in the ac susceptibility and noise spectrum at the frequency of the ac field that coincides with the frequency of the coherent oscillations of the antiferromagnetic sublattices [2-4]. Also, core size is correlated with superparamagnetic blocking temperature, with the magnetic stability of the magnetoferritin cores extremely sensitive to particle size. So, these magnetic, semiconducting, or conducting molecules are directly positioned in one- or two- dimensional arrays using scanning probe microscope (SPM)-based nanomanipulation to form a quantum computing logic gate.

Table I. Truth table for QCA majority gate.

Inputs			Output
A	**B**	**C**	**D**
0	0	0	0
0	0	1	0
0	1	0	0
0	1	1	1
1	0	0	0
1	0	1	1
1	1	0	1
1	1	1	1

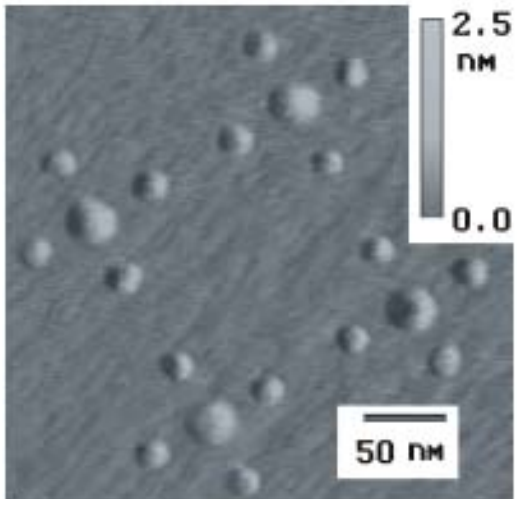

Figure 2. AFM image of a qubit-structured quantum dot array fabricated by the AFM lithography [10].

SPM-Based Nanomanipulator: Manipulation of the ferritin is required in nanometer-scale to arrange the quantum bits for quantum computing simulator. To construct quantum computing by using quantum dots, one of the biggest challenges is to materialize an ordered quantum dot array on a substrate with nanometer precision, because self-assembled quantum dots grown in the Stranski-Krastanov (S-K) mode are usually randomly organized. Self-assembly is sometimes capable of growing an ordered quantum dot array [19], but it is impossible to prepare differently sized quantum dots at the same time. And, quantum dots fabricated by electron beam lithography, which is one of the widely used techniques, are mostly still larger than 50 nm in diameter with an interdot distance above 100 nm, due to the proximity effect of the resist against electron beam [20,21]. The large lateral separation of quantum dots prohibit effective interdot coupling, which is fundamental in quantum computing created with quantum dots. Scanning tunneling microscope (STM) lithography was also used to fabricate self-assembled quantum dots [22]. The guiding element of the quantum dot position is introduced to the unexpected deposit and defect-rich growth of quantum dots inducing to the degradation of the quantum dot coherence, which is fatal in quantum computing. For this proposed work, scanning probe microscopy (SPM), especially atomic force microscopy (AFM), electrostatic force microscopy (EFM), magnetic force microscopy (MFM), current sensing AFM (CSAFM), and tunneling AFM (TUNA), are best considered due to their highest spatial resolution for visualization and tip modification. For the mechanical approach aspects, the tip needs to be able to find the material of interest and then push it into wanted position using the same probe, without damaging the material or the substrate. It should be possible to position magnetic ferritins attracted or repulsed to MFM tip. Alternatively, the ferritin molecule is positively charged as polycationic ferritins (PCFs) that should

be bound to an electrically polarized conducting tip. And, electrical signal through the patterned ferritin array is directly measured to the same tip using CSAFM or TUNA.

Selection of Candidate Materials and Preparation of Ferritins

The site-specific biomineralization within the shell enables the protein to be reconstituted with different core materials with different magnetic states (antiferromagnetic, ferrimagnetic, or superparamagnetic) and electrical properties (semiconductors with various band-gap and conductors with quantum confinement). The patterned ferritins can be formulated in terms of size and magnetic and electrical properties by self-assembling synthesis. Ferritins are considered promising candidates since they have a relatively large total spin S and high magnetic anisotropy [2-4,23]. The concept of quantum computing based on ferritin will open up numerous possibilities of applications such as the nano-reactor for the chemical fabrication of new materials, ultra high density data storage [24], quantum electronic devices [25], immunomagnetic cell label [26], biomedical nanorobots, magnetic refrigerator [27], tera hertz radiation source [8], etc.

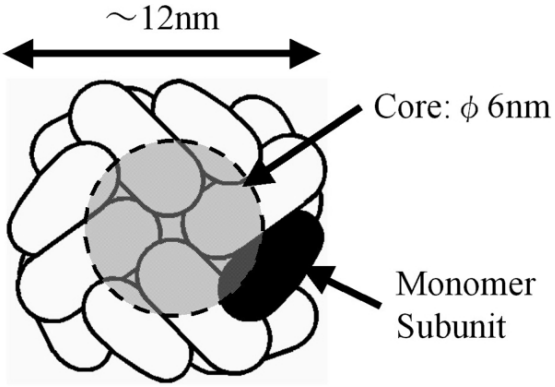

Figure 3. Schematic of the spherical shell of the ferritin protein.

Chemical Preparation: Ferritin is a natural iron storage protein that represents a high degree of structural similarity across a range of biological species as shown in Fig. 3. In natural ferritin, the core is composed of an antiferromagnetic iron oxide such as mineral ferrihydrite [1]. Ferritin protein has hydrophobic and hydrophilic molecular channels within the protein shell, which makes possible to remove the inorganic phase in vitro by reductive dissolution. The reconstitution of ferrihydrite cores in ferritin proceeds through subsequently remineralization of apoferritin. A synthesis of ferrimagnetic ferritin (γ-Fe_2O_3) was prepared by chemical remineralization procedure [17,18] with the assistance of H_2O_2 oxidant in 3-[(1,1-dimethyl-2-hydroxy-ethyl)amino]-2-hydroxy-propanesulsonic acid (AMPSO) buffer (pH 8.5) at 65 ^oC under N_2 gas. Biomineralization of some other metals in the ferritin cavity has been reported. Cobalt can be accumulated as a cobalt oxyhydroxide (CoOOH) state in the core with the aid of H_2O_2 oxidant [11]. Manganese also can be reconstituted in the cavity as manganese oxyhydroxide (MnOOH) by natural oxidation [12-14]. Nickel can be fabricated as nickel hydroxide ($Ni(OH)_2$) during the hydroxylation process of nickel ion solutions containing dissolved CO_2 and by precisely controlling the pH [15]. Cadmium sulfide [16] is one of the important candidates because many quantum computer schemes are based on semiconductor quantum dots [5].

Ferritin Immobilization on the Self-Assembled Monolayer-Modified Electrodes: Biologically derived nanoparticles can be fabricated from electrochemically-controlled biomineralization through the immobilization of ferritin on substrate. Immobilization of ferritin is achieved through the two different procedures. This process is very important to position precisely with ferritin molecules on conducting (Au, Pt, Ag, etc.) and Si substrates. One is the modification of substrate with thiol-derivatized molecules such as dithiobis-N-succinimidyl propionate (DTSP) and alkanethiols and then reacts with ferritin molecules. Another is the modification to the ferritin shell having thiol terminal group after chemical synthesis. The former method has two different approaches with different chemicals, but the reaction product is the same one. One is using a DTSP reaction and another is using a 1-ethyl-3-(3-dimethylaminopropyl)-carbodiimide hydrochloride (EDC) coupling reaction. DTSP is used as a protein cross-linking agent through acylation of free primary or secondary amino groups. DTSP also adsorbed onto gold surfaces through the disulfide group, so that the terminal succinimidyl groups are combined by amino-containing biomolecules [28]. The immobilization procedure begins with a cleaned polycrystalline gold electrode immersed in a 5 mM DTSP solution in dioxane for 1 hr at room temperature. Then the DTSP-modified electrode was thoroughly rinsed with acetone and finally with 25 mM N-[2-hydroxyethyly] piperazine-N'-[2-ethanesulfonic acid] (HEPES) buffer (pH 7.3). The DTSP-modified electrode was employed immediately after preparation to the 50 mM HEPES buffer solutions with 50 mM NaCl (pH 7.3) containing ferritin at a concentration of 2 mg/ml. The electrode was immersed in the ferritin solution for 18 hr at 4 ^oC and then rinsed with 25 mM HEPES buffer. Figure 4 showed a field emission-scanning electron microscopy (FE-

SEM) image of ferritin immobilized on DTSP modified Au electrode. Immobilized ferritin molecules are well isolated from each other on the Au electrode. We can clearly see the single molecule of ferritin with sphere-like protein shell having about 20 % coverage. It is gathered on the Au grain boundaries having the high surface energy while the physically adsorbed ferritins are well adsorbed on the gold electrode with a coverage of more than 60 % as shown in Fig. 5. We fabricated the mixed self-assembled monolayer (SAM) with DTSP and 3-mercaptopropanoic acid (MPA) or 6-mercaptohexanoic acid (MHA) for the preparation of isolated ferritin layer on the wholly passivated Au surface as shown in Figures 6, 7, and 8, respectively. The electrode was kept in the 1 mM DTSP solution containing with 10 mM MPA or (10 mM MHA) in dioxane for different times at room temperature. Immobilization of ferritin was achieved by immersion of the mixed SAM-modified electrode in the ferritin solution for different times at various temperatures. MPA has a same chain length compared to DTSP after reaction with ferritin while MHA has similar chain length to the anchored DTSP having suc-

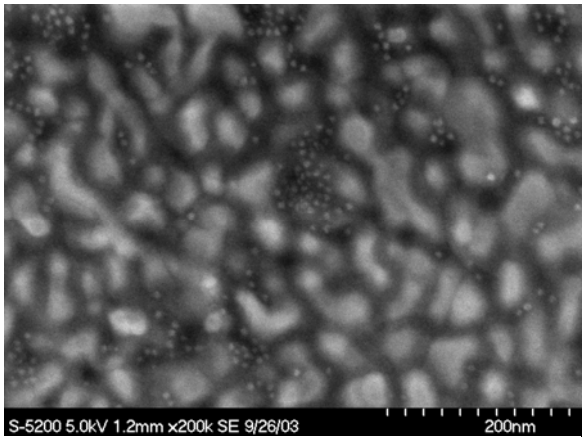

Figure 4. FE-SEM image of immobilized ferritin on DTSP-modified Au.

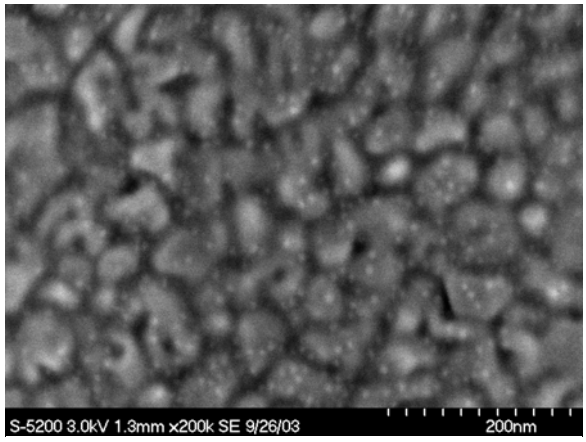

Figure 5. FE-SEM image of physically adsorbed ferritin on Au.

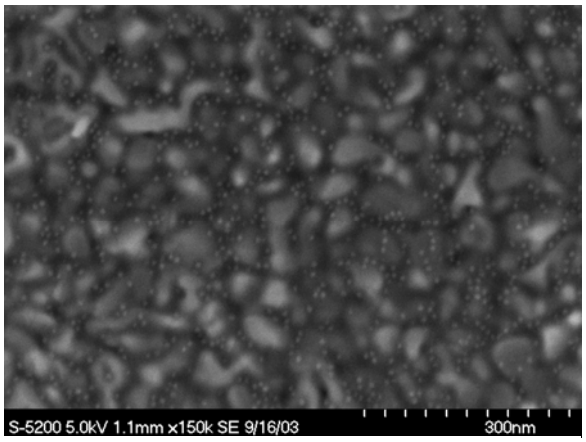

Figure 6. FE-SEM image of immobilized ferritin on DTSP and MPA-modified Au. Mixed SAM is adsorbed on Au for 1 hr at room temperature. And then, DTSP and MPA-modified Au is inserted immediately into the ferritin solution for 18 hr at 4 ^{o}C.

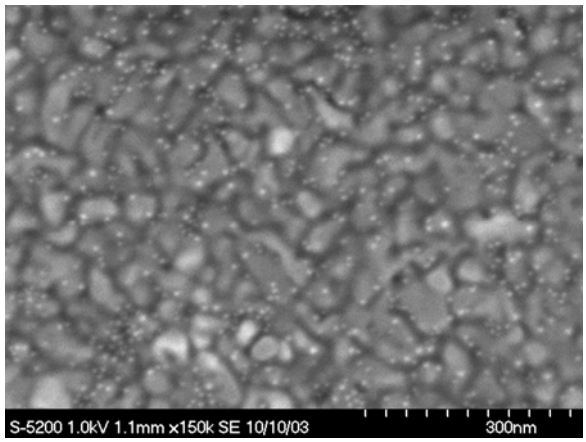

Figure 7. FE-SEM image of immobilized ferritin on DTSP and MHA-modified Au. Mixed SAM is adsorbed on Au for 1 hr at room temperature. And then, DTSP and MHA-modified Au is inserted immediately into the ferritin solution for 18 hr at 4 ^{o}C.

cinimidyl group. The ferritin molecules immobilized on the DTSP and MHA-modified electrodes for 18 hr have the highest population after the dipping for 2 hr in ferritin solution at room temperature (Fig. 8). The reaction rate between the ferritin and DTSP increases as the reaction temperature increases.

Another immobilization method using Au surface modification is using an EDC coupling reaction between the carboxyl terminal groups of pretreated mercaptopropanol SAM on gold and the amino groups of ferritin shell. All of these reactions are carried out in 4-morpholinoethanesulfonic acid (MES) buffer solutions between pH 4.5 to 5.0 reacting with N-hydroxysuccinimide (NHS) molecules. We can get the same results of immobilized ferritin prepared by DTSP modification with three carbon chains. But, this approach is very important to fabricate the patterned ferritin arrays using SPM-based nanomanipulation. Now, we can control the site and coverage of immobilized ferritins through the above methods with DTSP and/or ferritin dipping time, dipping temperature, and ratio of DTSP and passivating molecules in the solution.

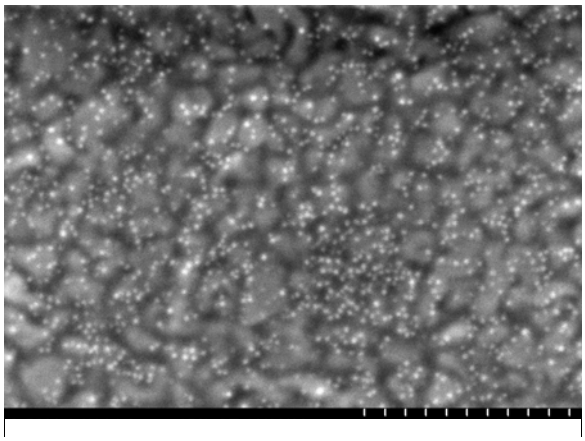

Figure 8. FE-SEM image of immobilized ferritin on DTSP and MHA-modified Au. Mixed SAM is adsorbed on Au for 18 hr at room temperature. And then, DTSP and MHA-modified Au is inserted immediately into the ferritin solution for 2 hr at room temperature.

We can immobilize the ferritin molecule on gold through the modification onto ferritin shell with thiol group. We used a procedure for protein thiolation based upon a method described by Traut et al.[29,30]; the free thiol groups which are introduced bind to the gold surface, immobilizing the protein molecule. Thiolation of ferritin using Traut's reagent is described in Fig. 9. First, a buffer solution was prepared (triethanolamine hydrochloride buffer) consisting of triethanolamine hydrochloride (50 mM), KCl (50 mM), and $MgCl_2$ (1 mM). Second, a stock solution was prepared immediately before use consisting of 2-iminothiolane (0.5 M) triethanolamine hydrochloride (1.0 M), and triethanolamine (1.0 M), with a pH of 8.0. The reaction mixture was prepared as follows: 77.73 µl of ferritin (77 mg/ml), 200 µl of mercaptoethanol, and 24 µl of the stock solution were placed in a vial and diluted to 20 ml with triethanolamine hydrochloride buffer. The reaction was then incubated for 20 min at 0 °C. After completion, the reaction was quenched by reducing the pH to 4, and the excess reagent was removed by dialysis against 100 volumes of triethanolamine hydrochloride buffer at 4 °C for 4hr. Then the mixture was diluted by a factor of 100 in phosphate buffer (pH 7.8). Adsorption of the thiolated ferritin was performed by inserting a Au substrate into the solution for 18 hr. Figure 10 shows FE-SEM images of thiolated ferritin on Au. We can get the highly packed and well-dispersed monolayer of ferritin using the thiolation of ferritin. All gold surfaces are covered by thiolated ferritin and the size of single ferritin molecule is about 12 nm diameter (see Fig 10b).

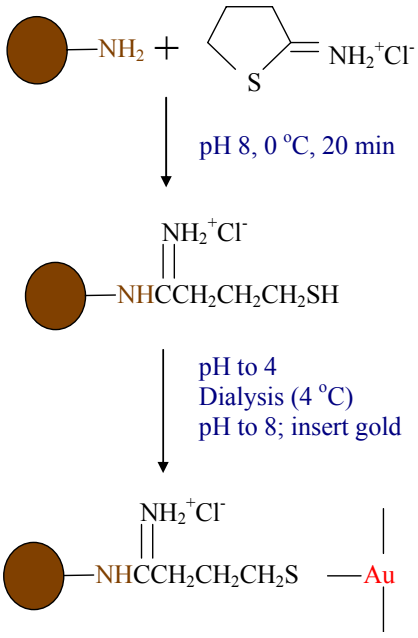

Figure 9. Schematic diagram of ferritin thiolation.

NanoManipulation of Ferritin Molecules

The NanoMan system used as nanomanipulator in this proposed work is the most advanced system commercially available for nano-scale surface modification. It provides extremely accurate control of the in-plane position and movement of the SPM probe for direct, precise manipulation of nanoparticles and other nano-scale objects, as well as for high-definition nanolithography. Several approaches to achieve the exact positioning of ferritin are being explored, they include mechanical, chemical, and diluted electro/magneto precipitation (DEMP) methods using a SPM-based nanomanipulator.

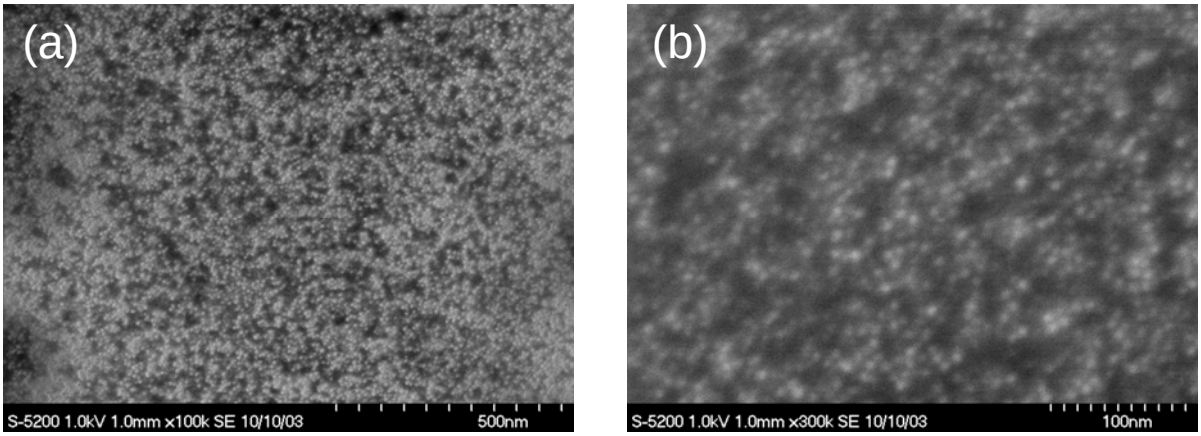

Figure 10. FE-SEM images of thiolated ferritin on Au: (a) ×100 k and (b) ×300 k.

Mechanical Approaches: NanoMan is used as an x-y positioning tool for the ferritin movement and the sharpened silicon tip is used as a "nano-finger" for ferritin dribbling to build new a patterned structure such as the proposed quantum logic gate. The mechanical method performed with the well dispersed ferritin molecules on mica or a silicon substrate. First, we tested the adsorption properties of ferritin on mica and Si surfaces. Figure 11 shows a FE-SEM image of well dispersed holo ferritin molecules on Si substrate. A cleaned Si substrate was immersed into the ferritin solution (concentration of 2 mg/ml) for 3 min. The adsorbed ferritin molecules are well separated from each other with a size of 12 nm. We can isolate the ferritin molecules using a simple dipping method with the interdot distance between ferritin molecules of about 50 nm. Mica has an atomically flat, electrically insulating, and negatively charged surface. In this case, we used cationic ferritin, which prepared by coupling ferritin from HoSF with N,N-dimethyl 1,3-propanediamine (DMPA), for strong adsorption onto negatively charged mica surface. We changed to the engaged tapping force from soft to hard for the separation between ferritin shell and core metal as shown in Fig. 12, 13, and 14. The core size of ferritin molecule decreases as the tapping force increases. The diameter and height of single dot are about 40 nm and 6 nm, respectively, due to the convolution effect of relatively huge tip. As you can see, the core metal distinguished from the surrounded protein (dark parts) with white spot at the center of ferritin dot in the phase detection image (see Fig. 13b). Figure 15 shows tapping mode AFM images of physically adsorbed ferritin on Si substrate depending on the dipping time. The population of ferritin can be not distinguished from samples prepared for 0.5 and 1 min dipping while the samples prepared for 5 and 10 min dipping have an almost packed layer with aggregates to some degree. We tested to move the adsorbed ferritin mechanically on the two different substrates such as mica (insulator) and n-doped Si (almost conductor) using the nanomanipulator. Figure 16 shows the linear positioning of ferritin molecules on mica substrate constructed by the mechanical pushing with silicon tip. The atomically flat surface of mica was inserted into the aqueous solution containing ferritin at a concentration of 2 mg/ml for 1 sec. We positioned the three big dots at upper, center and lower left corner of the image. We moved the dots following the arrows in the feedback off conditions with z distance of – 40 nm, z velocity of 60 nm/s, and xy velocity of 2 μm/s. When we engaged to the different parameters with larger z distance of – 50 nm and xy velocity of 4 μm/s, the one dot is divided to the two dots (see Fig. 16d and e). The big dot of upper center may be

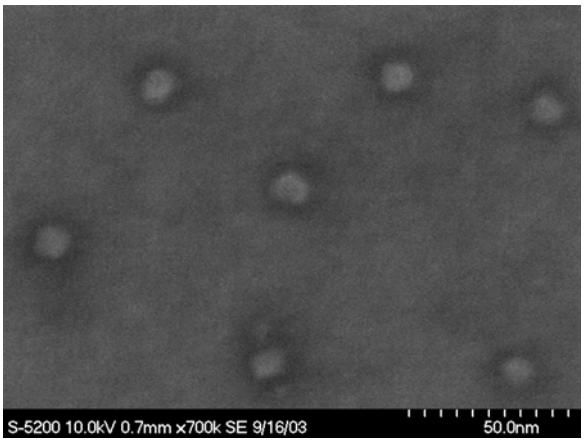

Figure 11. FE-SEM image of physically adsorbed ferritin on Si for 3 min.

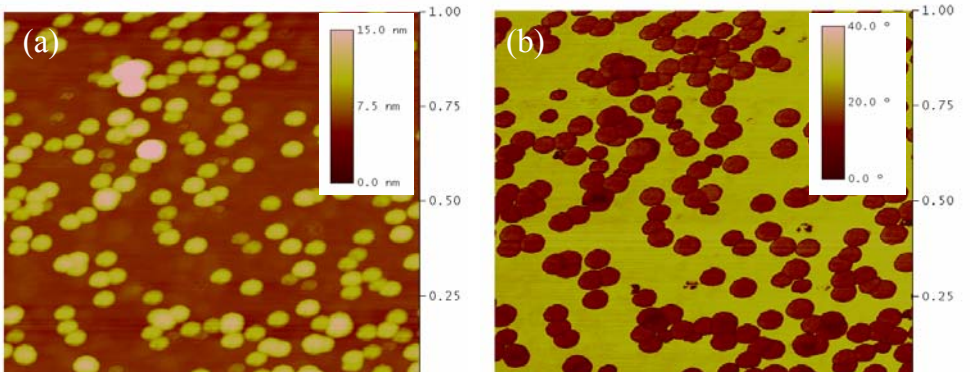

Figure 12. (a) AFM and (b) PDM images of physically adsorbed cationic ferritin molecules on mica substrate for 3 sec using soft tapping force.

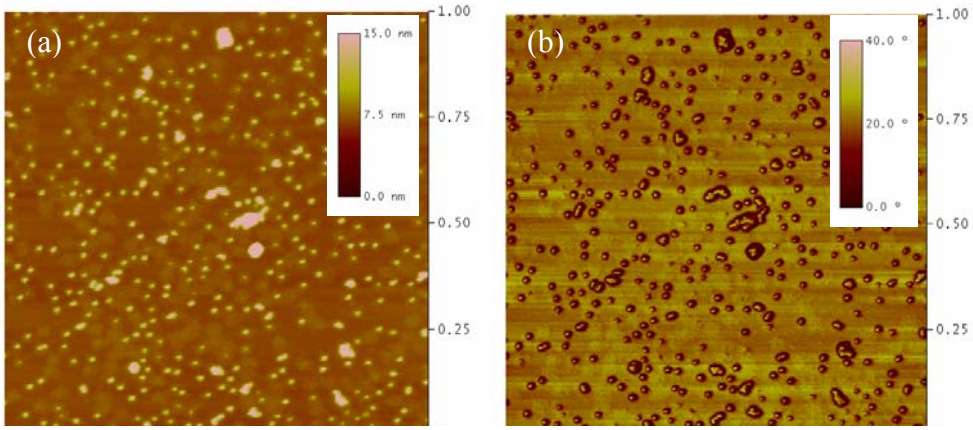

Figure 13. (a) AFM and (b) PDM images of physically adsorbed cationic ferritin molecules on mica substrate for 5 sec using medium tapping force.

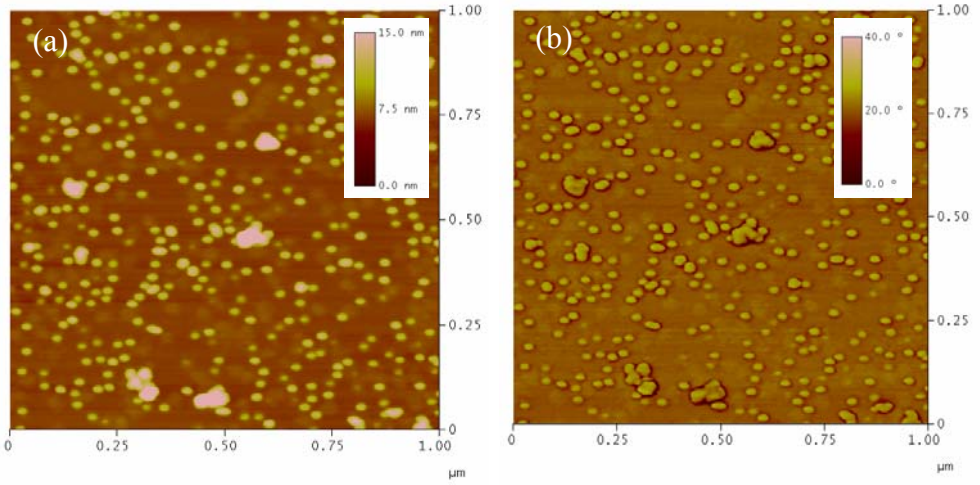

Figure 14. (a) AFM and (b) PDM images of physically adsorbed cationic ferritin molecules on mica substrate for 5 sec using hard tapping force.

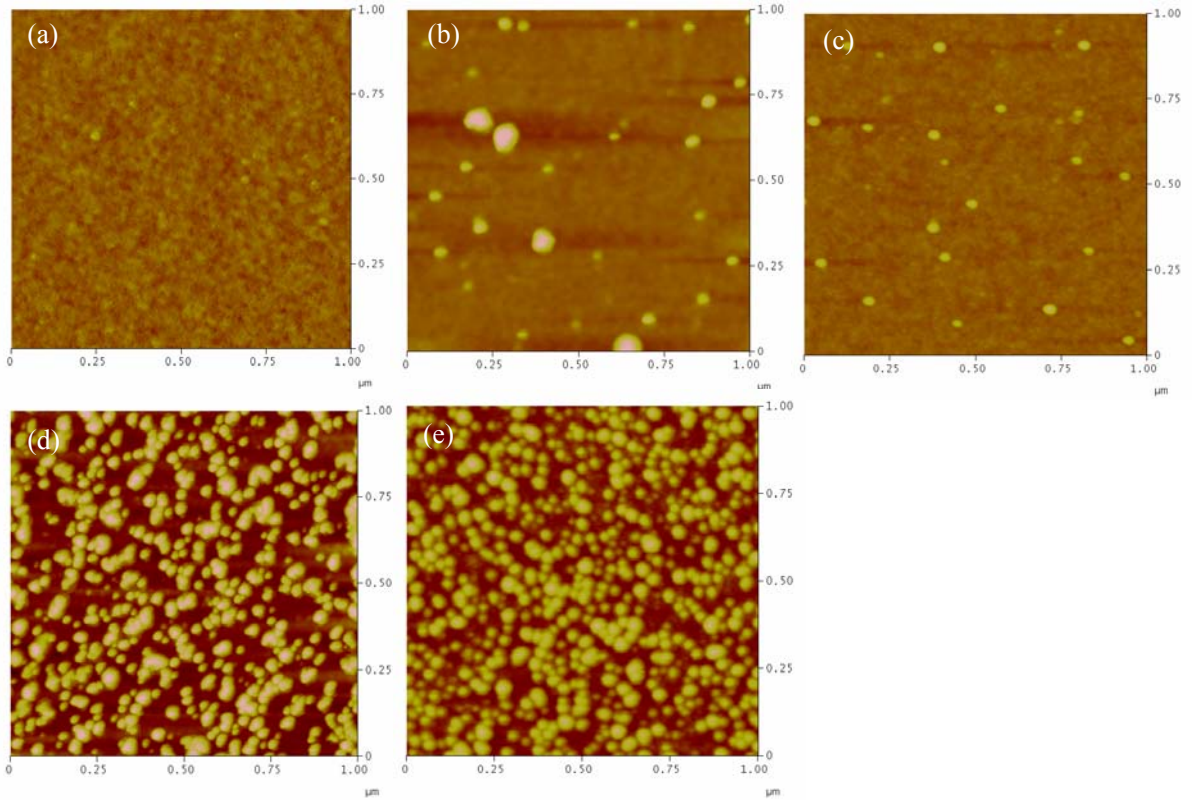

Figure 15. Tapping mode AFM images of physically adsorbed ferritin on Si substrate for (a) 0 min, (b) 0.5 min, (c) 1 min, (d) 5 min, and (e) 10 min.

aggregate of ferritins. So, this is not the protein destruction at the vigorous condition, but only division of ferritin aggregates.

Second of ferritin manipulation tested on cleaned Si substrate. The Si substrate was immersed into the piranha solution (H_2SO_4 : H_2O_2 = 70 : 30 vol.%) for 5 min in four times. Cleaned Si substrate was washed with flowing double distilled deionized water and then dried with nitrogen gas for 10 min. Cleaned Si substrate was inserted into the ferritin solution of 2 mg/ml concentration for 30 sec. The manipulation parameters were set as the tapping mode with feed back using closed roof for the precise location of tip without scanner drift in the imaging mode, but the manipulation mode was operated at the feed back off condition with z distance of – 60 nm, z velocity of 60 nm/s, and xy velocity of 4 μm/s. We could dribble the ferritin molecules with silicon tip at above conditions. We could make the heptagon shape-patterned array with one dot at the center. In this approach, we have a problem that the protein shell is adsorbed on the Si tip. Sometimes, we cannot see the ferritin molecules after manipulation. Therefore, we need to modify the surface of substrate or tip with the positively or negatively charged molecules, or to find different approaches for patterning with ferritin. Now, we proposed the chemical approaches and diluted electro/magneto precipitation (DEMP) methods to fabricate the quantum dot arrays.

Chemical Approaches: We designed the conceptual schemes for nanopatterning of ferritins using SPM-based technology. Nanofabrication of quantum dot arrays for quantum logic gates will be achieved by follows as: (1) the site-specific immobilization of thiolated ferritin onto the AFM tip induced local point oxidation (see Fig. 18), (2) the ferritin location induced by gold nanoparticle manipulation (see Fig. 19), and (3) in-situ ferritin positioning using shaving method (see Fig. 20). Nano-scale site- specific immobilization method will be achieved with SAM of 3-mercaptopropyl-trimethoxysilane (3-MPTMS) on the Si substrate. 3-MPTMS reacts with terminal hydroxyl groups on the cleaned Si substrate pretreated with piranha solution using gas phase [31]

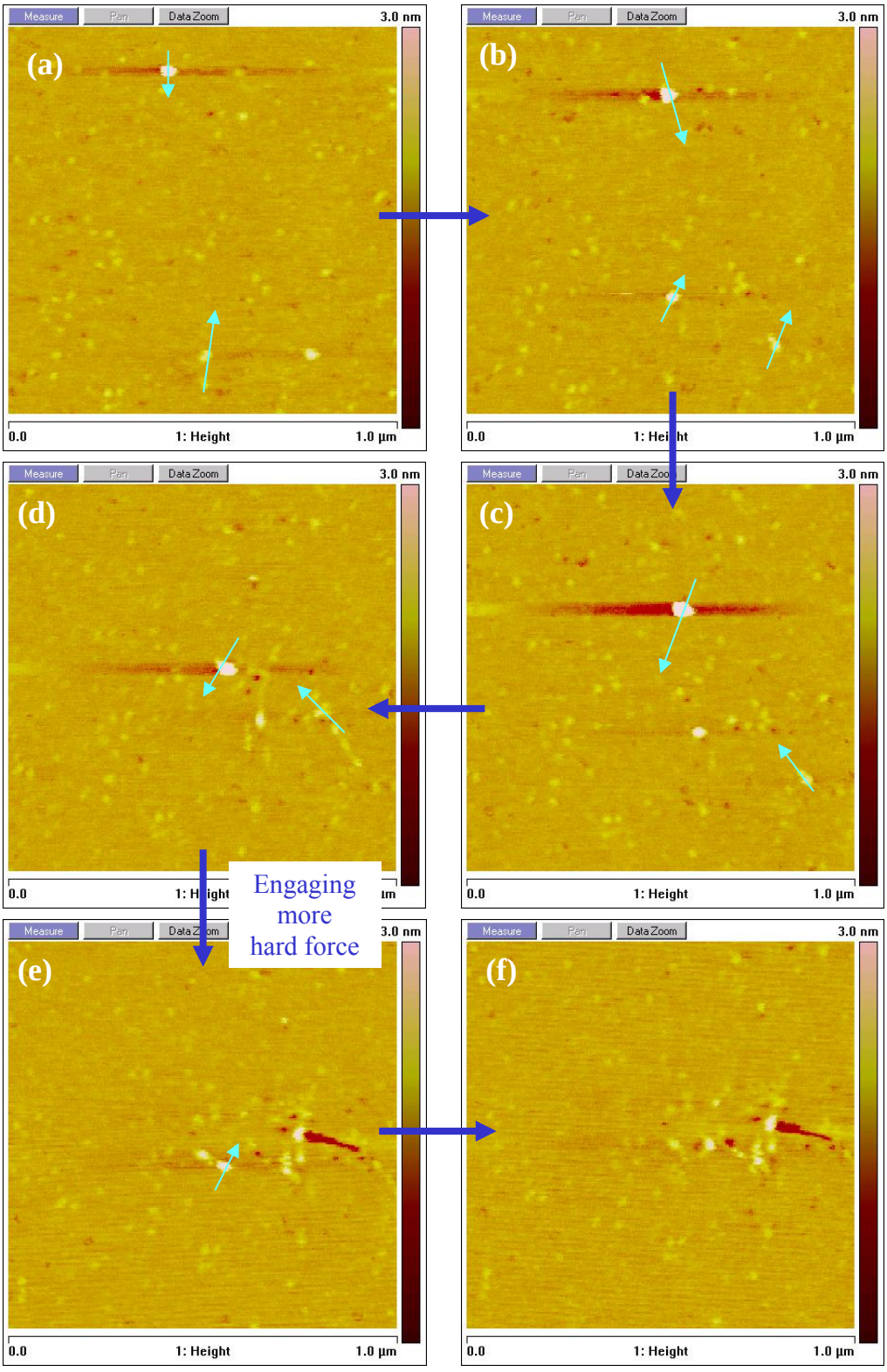

Figure 16. Mechanical nanomanipulation of ferritin molecules on mica substrate.

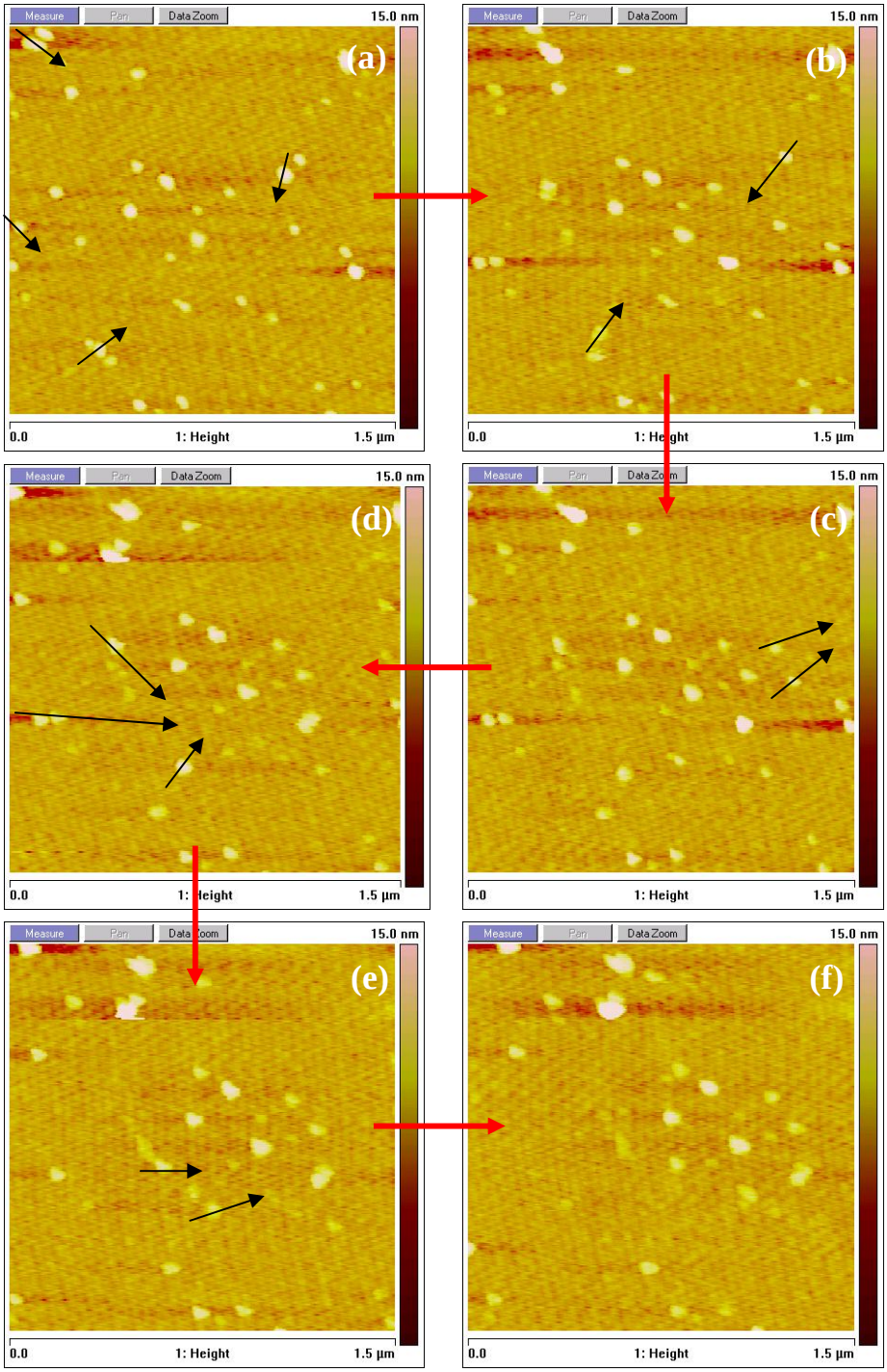

Figure 17. Mechanical nanomanipulation of ferritin molecules on Si substrate.

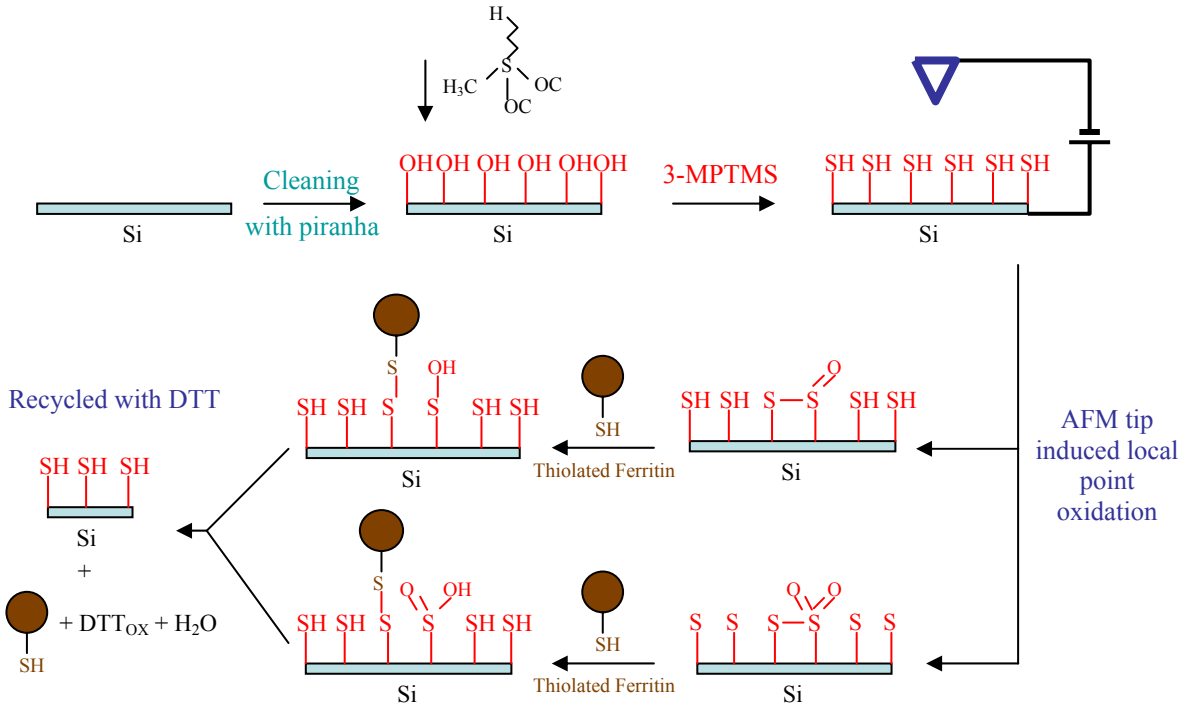

3-MPTMS: 3-mercaptopropyltrimethoxysilane, DTT: Dithiothreitol

Figure 18. Schematic diagram of nano-scale site-specific immobilization of thiolated ferritin.

or solution phase reaction [32]. Now, Si surface is modified to the terminal thiol groups. Electrochemical oxidation of the thiolated surfaces will be achieved under ambient conditions using the SPM-based nanomanipulator in contact mode. To optimize the achieving potential, different potential will be applied between the conducting tip and the surface. The NanoMan will be used to control tip movement, drawing patterns at a different speed of tip moving while closed roof and applying the potential difference. Thiols are electrochemically oxidized to thiosulfinates or thiosulfonates by applying a potential difference between AFM tip and thiol-derivatized surface. Nano-patterning of ferritin molecules will be realized through immobilization of thiolated ferritin onto the localized patterns of oxidized thiols. And, this can be a rewritable process by treatment with dithiothreitol (DTT).

Second approach is gold nanoparticle induced ferritin manipulation as shown in Fig. 19. Gold nanoparticles with size ranges of 5 to 10 nm will be dispersed on cleaned Si or cleaved mica substrates. Gold nanoparticles are manipulated to the designed quantum logic gate using the SPM-based nanomanipulator and the same method of mechanical dribbling technique. The patterned ferritin array can be accomplished with immobilization of thiolated ferritin onto the previous patterned gold nanoparticles.

Third method is in-situ ferritin immobilization on passivated gold surface using shaving method as shown in Fig. 20. The gold surface is modified with long chain alkanethiol such as decanethiol, hexadecanethiol, etc. Nano-patterns will be produced by the mechanical scratching with high contact forces in the thiolated ferritin solution or dithiobis(sulfosuccinimidyl) propionate DTSSP solution that is a water soluble form of DTSP. When the high forces are engaged on the long chain alkanethiols, thiolated ferritin or DTSSP molecules are adsorbed onto the cleaved alkanethiol site. We can easily attain the nano-patterned arrays of ferritin. All three of them are next year approaches to complete for the ferritin based quantum logic gate.

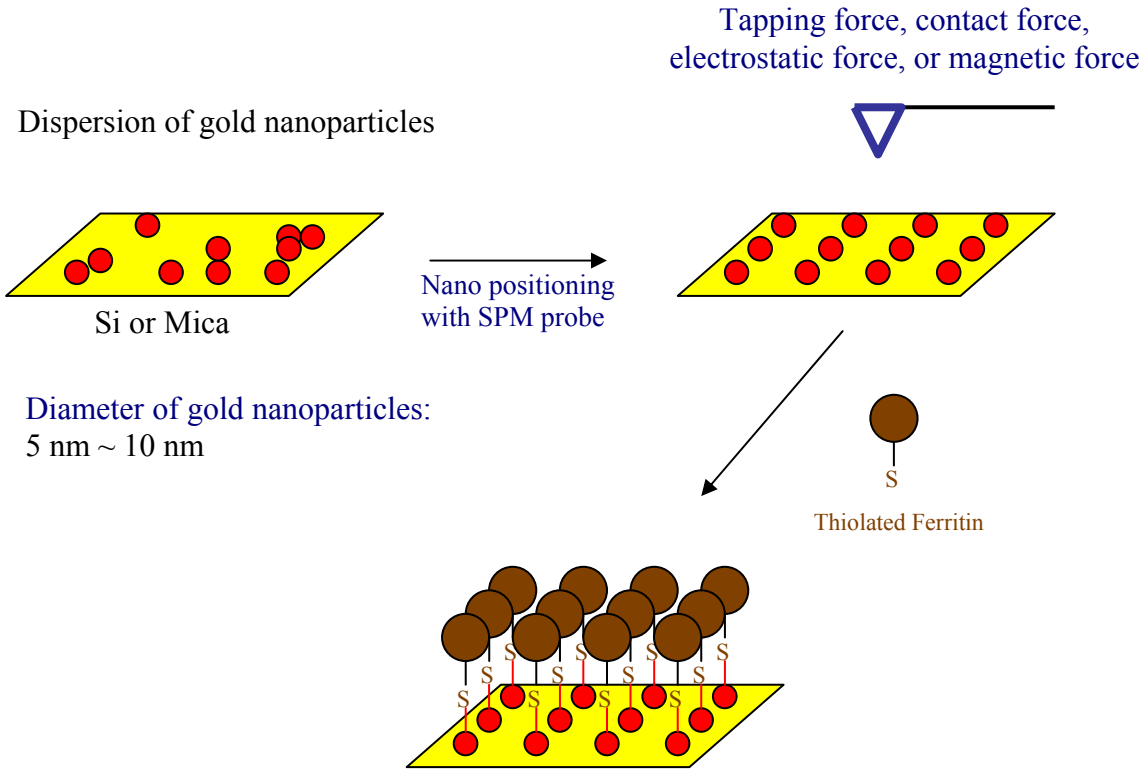

Figure 19. Schemicatic diagram of gold nanoparticle induced ferritin manipulation.

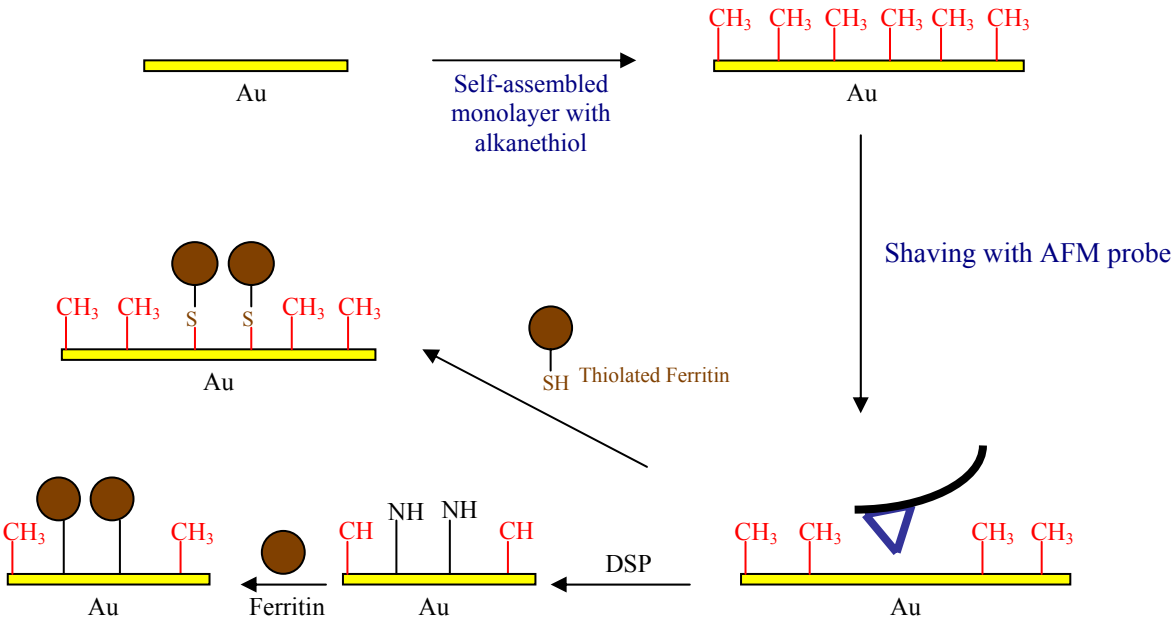

DTSSP: dithiobis(sulfosuccinimidyl) propionate

Figure 20. Schematic diagram of in-situ ferritin positioning using shaving method.

Diluted Electro/Magneto Precipitation (DEMP) System: The main purpose is to deposit and position each ferritin precisely to a desired location on the substrate as shown in Fig. 21. The concentration control of ferritin suspension is key factor for initializing the DEMP process. The ferritins within the body of solution are sparsely populated, so that the submerged tip of AFM does not disturb ferritins in a colloidal suspension. In such a dilution process, the tip stays down with sufficient distance from the ferritins and prevents ferritins from attaching to the AFM tip. Direct positioning of a ferritin onto the desired location is possible by the repeated pulse of field applied through the conducting or magnetic tip that attracts the nearest ferritin a little bit of distance. The strength of applied field required for the attraction of a ferritin molecule must be sufficiently large enough to overcome the electrical or magnetic attraction among ferritins, viscous drag of a solution, and the random thermal agitation, thus resulting in Brownian motion. Although the time of flight is constant over the repeated pulses, the travel distance of a ferritin increases along with each repeated pulse of applied field since the field strength becomes higher at a closer distance. Eventually, a ferritin is attracted, arrives at and sticks to the AFM tip. Next, a ferritin is pushed by the pulses of reverse field while being pulled by the localized and narrow field beneath the substrate to a designated position. The DEMP process offers an effective nanofabrication capability that will be very useful for developing nano-devices based on quantum dots.

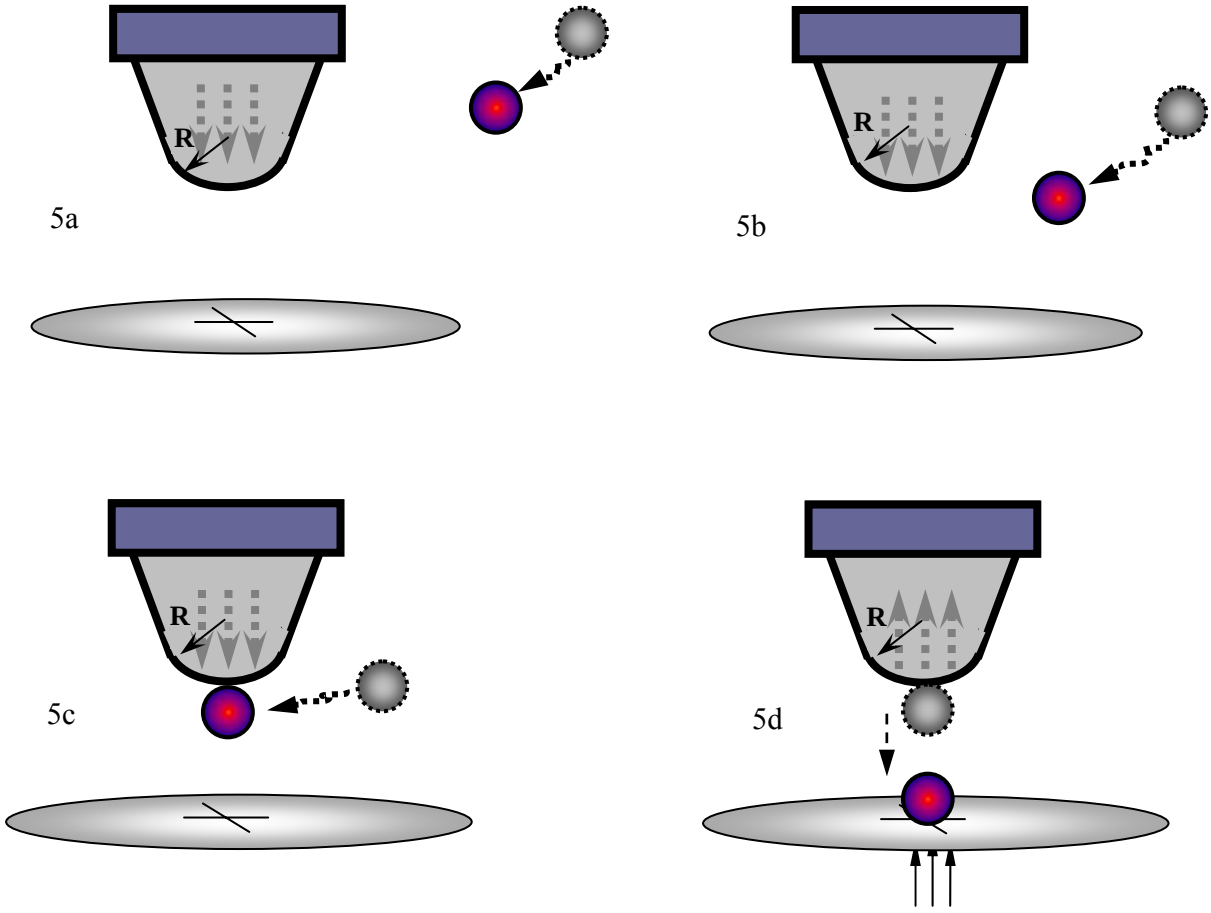

Fig. 21 Positioning steps of nanoparticles in solution using Diluted Electro/Magneto Precipitation (DEMP) System

Signal Measurements of QLG

The electrical and magnetic properties of single ferritin molecule and apoferritin were measured in isolated ferritin thin layer using CSAFM and MFM, respectively. The respective SPM tips act as a "nano-finger" to both sense the signal and manipulate the ferritin molecules. Conventional measurements of quantum computing signal are conducted by a superconducting quantum interference device (SQUID), nuclear magnetic resonance (NMR), or Mössbauer spectroscopy. These techniques are operated in extreme conditions and showed total

quantum mechanical signals. But, SPM-based measurements used in this work supported to the local signals and the surface electrical and magnetic signal mapping.

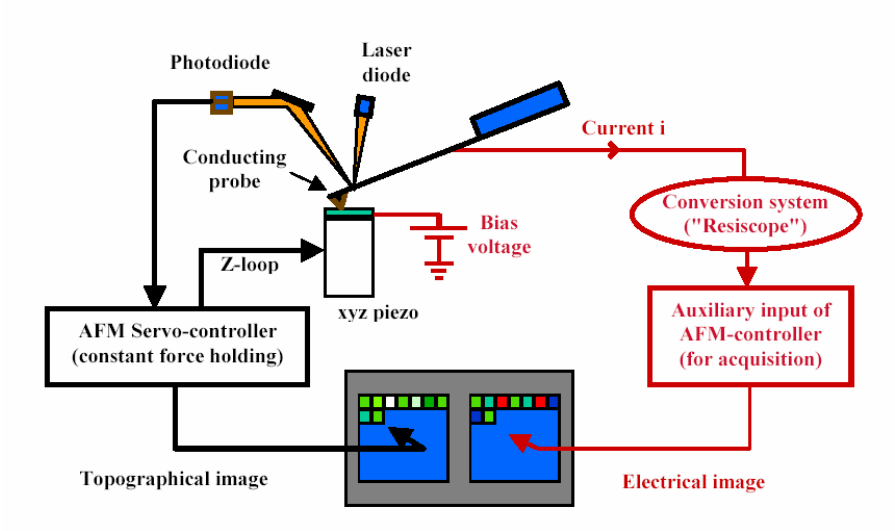

Figure 22. Schematic diagram of CSAFM.

Electrostatic Field Transmission: In this work, we used a CSAFM technique for measurement of electrical property of single ferritin molecule with a conducting tip applying voltages between the conducting tip and sample as shown in Fig. 22. This technique used a conducting tip coated with gold, platinum, and boron-doped diamond film for measuring and applying current and potential, respectively. The conducting tip is positioned at the exact position on the substrate and then contacts with known contact force. *I-V* curve or surface current image is obtained through measuring the current between the tip and sample for potential sweeping or engaging to the constant potential. This technique has a lot of advantages measuring of electrical property without pretreatment or separation of arrayed molecules on the substrate, controlling the precise position with closed roof module, and controlling the contact force between the tip and ferritin molecule. CSAFM has a lateral resolution of less than 0.1 nm and a vertical resolution of less than 0.01 nm.

Topography and current- voltage (*I-V*) characteristic curve measurements of both holo and apoferritin single molecule were carried out using CSAFM as shown in Fig. 23. A sharpened Au-coated conducting tip was employed for both measurements. AFM image and *I-V* curve were measured at a low contact force less than 10 nN in a contact mode preventing possible damage of probe tips and samples. Both the topography and electrical measurements were performed using the same tip. For *I-V* measurements, current was measured at various bias voltages applied between the conducting tip and contact layers using current sensing module. All measurements were performed at room temperature under flowing nitrogen purge gas in a chamber. Each *I-V* characteristic curve was plotted by measuring 20 times and averaging the data. Figure 24 shows *I-V* characteristic curves of holo and apoferritin using CSAFM. For these measurements, a metal/biomolecule junction was formed by placing an Au-coated conducting tip on an individual ferritin molecule surface as shown in Fig. 23. A typical *I-V* curve for the holo ferritin molecule (Fig. 24 (a) and (b), respectively) on atomically flat gold surface reveals the expected current rectifying behavior with turn-on voltages at ~ + 0.5 V and – 0.5 V for forward and reverse biases, respectively, while the turn-on voltages of apoferritin appear at ± 1.0 V. The *I-V* characteristic curves for the point contact on ferritin represent nonlinear and symmetric behavior although the detailed shape of the curves depended on surface conditions as well as measurement parameters, e.g., the contact force of the tip. The similarity between numerical values of the turn-on potentials is in reasonable agreement with the same work function of Au (~ 5.3 eV) between the tip and substrate. The operating voltage is about 1.0 V and 2.0 V for holo

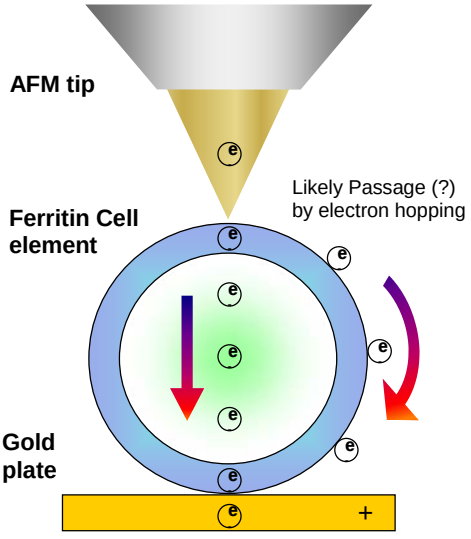

Figure 23. Schematic diagram for the electrical property measurement of ferritin single molecule.

and apoferritin, respectively. Holo and apoferritin have a similar behavior of semiconducting material with small band gap. The electron transport mechanism takes place either by tunneling through the ferritin shell, or by hopping on the surface. The *I-V* curves show quite satisfactory linearity in Fowler-Nordheim [$ln(I/V^2) \propto 1/V$] coordinates (not shown). The electrical properties of holo and apoferritin followed to the Fowler-Nordheim tunneling model with a larger tunneling barrier height for apo than holo ferritin.

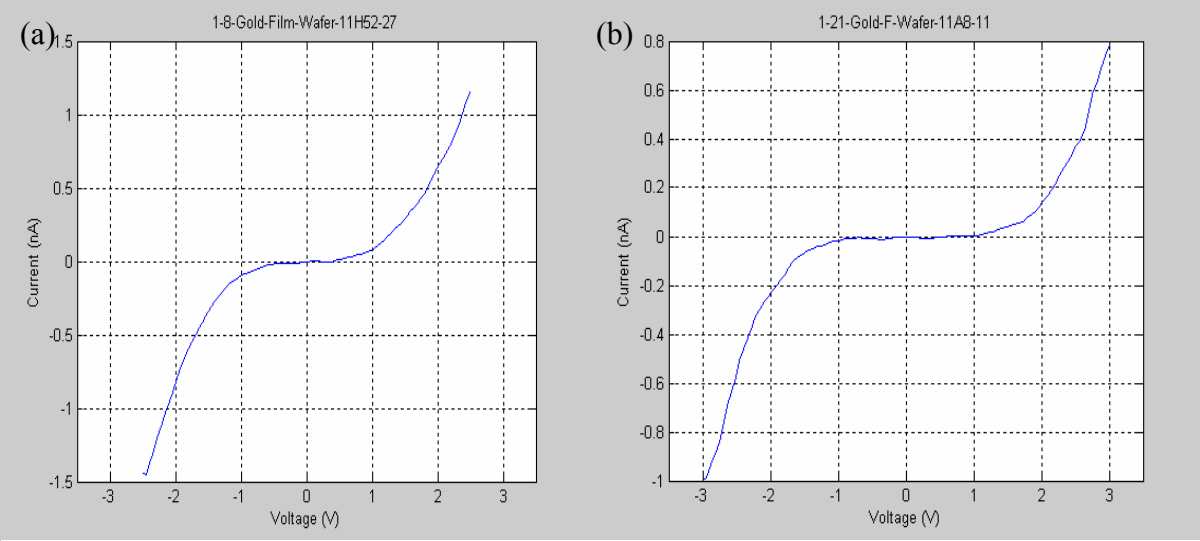

Figure 24. Typical I-V curves of (a) holo and (b) apoferritin using CSAFM.

The patterned ferritin arrays will be fabricated on an insulator (e.g., mica), silicon, or SAM-modified gold substrate with one input micro-scale electrode. Input signals are engaged through the e-beam patterned electrodes and output signal passing through the patterned ferritin array will be detected through the conducting tip located on the local ferritin molecule. Also, we can change the gate voltage of substrate operating the quantum logic gates.

Magnetic Spin Measurements: Another choice of quantum computing signal detection measures a magnetic spin or force of local ferritin molecule. The magnetic force microscopy (MFM) based on SPM technique operates in a lift mode whereby a single scan line is taken to determine the topography in tapping mode, followed by a repeat scan where the tip is lifted a fixed distance above the surface. This second scan records the long-distance forces acting on the probe due to the magnetic field gradient above the patterned ferritin arrays. Typical lift heights were on the order of 10 nm and could be adjusted to give better contrast. The tip was cobalt coated sharpened silicon nitride cantilever with an approximate radius of curvature of 60 nm. Lateral resolution is on the order of 20 nm for this lift mode procedure. Although, this may seem poor, the ability to resolve and ability to see are not mutually exclusive. The magnetic properties of localized ferritin will be measured as a function of the magnetic frequency from 50 MHz to 1 GHz or magnetic field from 600 Oe to 15000 Oe. The zero-field maximum in the dependence of the magnetic relaxation rate on the magnetic field in ferritin will be observed for resonance tunneling of magnetization in patterned ferritin layers. Also, the MFM probe can be used as a field source that excites the magneto-resistive property in a core of ferritin molecule. The current through the biased sensor will become to vary in response to the oscillating MFM tip. So, we can investigate the symmetry and sensitivity of patterned ferritin layers.

Electrochemical/Chemical Biomineralization of Ferritins with Different Core Materials. Apo ferritin was prepared by the reductive dissolution of native iron oxide cores of holo horse spleen ferritin (HoSF, Sigma) using the thioglycollic acid procedure.[33] Apo HoSF was further reacted with dithionite in the presence of bipyridine to remove iron. Protein concentrations were determined by the Lowry method and confirmed by the absorbance at 280 nm which is a specific amino acid absorption peak.[34] Co and Mn oxyhydroxide mineral cores were fabricated within the ferritin interior.[35,36] Apoferritin solution prepared in the above procedure was adjusted to a proper pH level with 0.01 M NaOH. $Co(NO_3)_2$ (25 mM, 80 μl) was used as a cobalt source

and added to apoferritin solution, followed by addition of excess amount of H_2O_2 (3 vol.%, 40 μl). Co addition was conducted over 2 hr period with 10 min intervals, maximizing metal loading. Just before Co ferritin started to precipitate due to excess Co loading, the reconstitution reaction was stopped by adding 3 μl of catalase. In this work, the amount of Co loading was measured to be 1000 Co per ferritin molecule. According to spectroscopy results, Co atoms loaded inside ferritin exist as Co(III)-oxyhydroxide, CoOOH.[11] Higher Co loadings can be attained but the reaction becomes slow and the yield decreases because of protein precipitation as the core approaches its theoretical limit of 4000 Co per ferritin. This ferritin reconstitution can be basically applied to any other metal loadings. Manganese also can be reconstituted in the cavity as manganese oxyhydroxide (MnOOH) by natural oxidation. Also, nickel can be fabricated as nickel hydroxide ($Ni(OH)_2$) during the hydroxylation process of nickel ion solution that requires dissolved CO_2 and a precise pH control.[15] Figure 25 shows scanning transmission electron microscopy (STEM) images of Fe-, Co-, Mn-, and Pt-cored ferritins developed herein. These are good candidates as a QD for signal transport and storage to develop QLGs. We can easily control the number of metal atoms in the ferritin interior. Each ferritin has a 2000 Fe, 1000 Co, 1000 Mn, and 200 Pt atoms per ferritin, respectively. Metal cores are evenly distributed in the ferritin interior and have good size similarity. The size of core depends on the number of metal atoms inside ferritin.

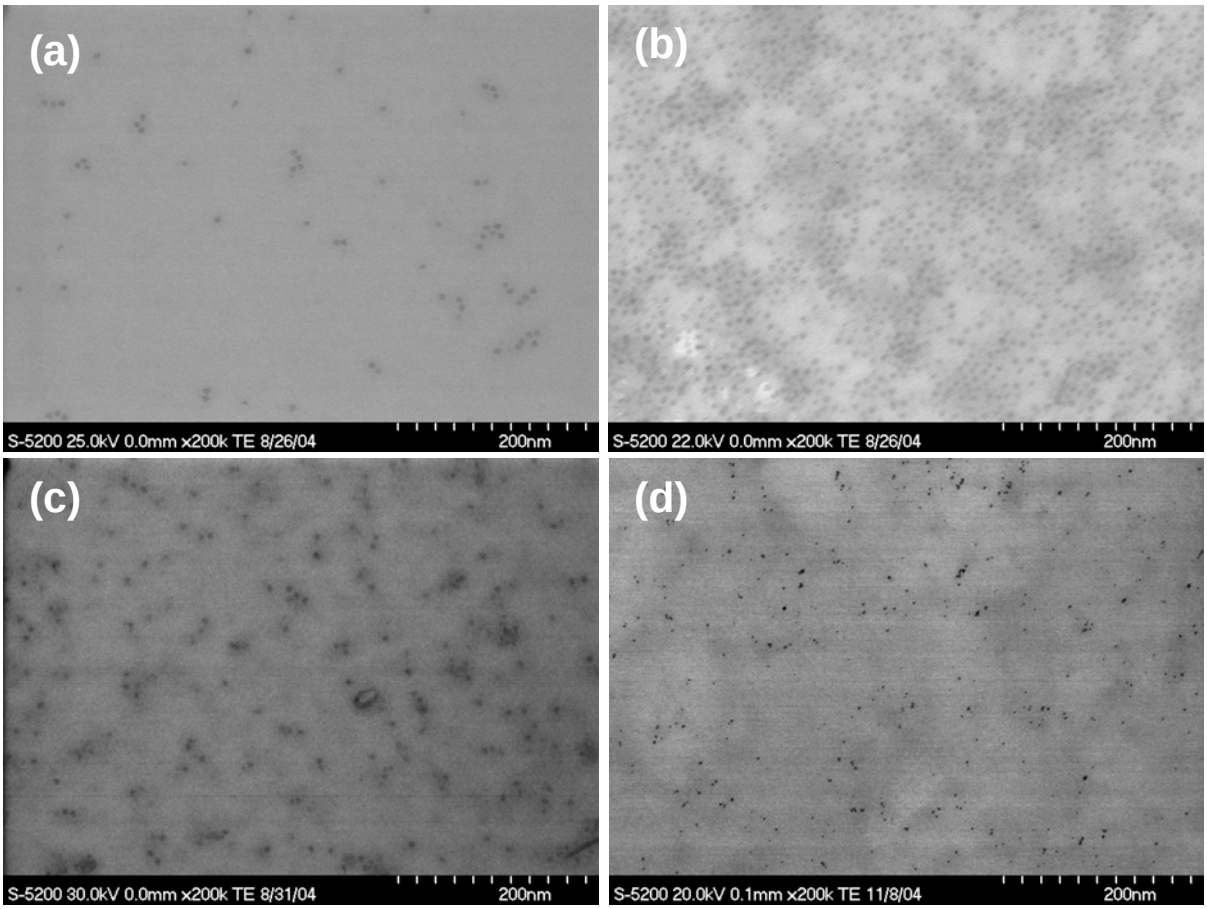

Figure 25. STEM images of chemically prepared (a) Fe-, (b) Co-, (c) Mn-, and (d) Pt-cored ferritins. STEM images were taken after addition of 2000Fe^{2+}, 1000Co^{2+}, 1000Mn^{2+}, and 200$PtCl_4^{2-}$ into an apoferritin, respectively.

Measurement of Electronic Conductivity. Two methods were used to measure conductivity of the ferritin molecules adsorbed onto a gold substrate. The first method was a single molecule measurement made with an Atomic Force Microscope (AFM) probe. A 20 nm gold coating was deposited on the silicon AFM probe tip(s) used for the measurements. The AFM tip was positioned on a ferritin molecule and the current through the ferritin molecule was measured vs. the voltage applied between the tip and the gold substrate. Typical experimental results are shown on Figure 26 for holoferritin (with a ferrihydrite core) and apoferritin (with an empty core).

The current observed at a given potential was considerably higher for the holoferritin than the apoferritin. The measured resistance near zero bias was 1.8 T ohms for holoferritin and 5.7 T ohms for apoferritin. Hence, the conductivity of holoferritin was about 3 times higher than the conductivity of apoferritin, leading to the conclusion that most of the holoferritin current passed through the ferritin core rather than through the protein shell.

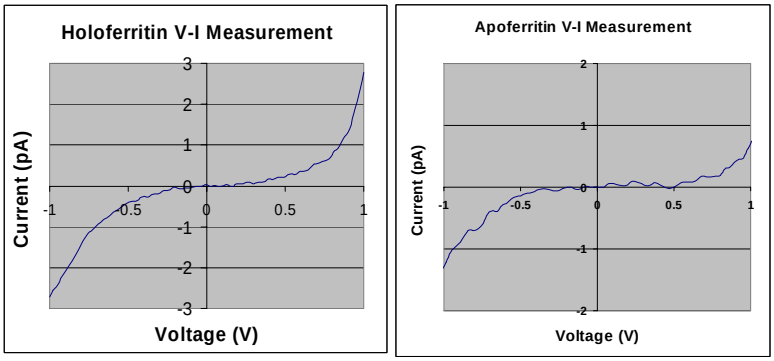

Figure 26. I-V behavior of single iron-ferritin molecules: a) holoferritin b) apoferritin.

The AFM based measurements provided conductivity measurements on single ferritin molecules. Repeated measurements of the conductivity on the same ferritin molecule yielded similar results. In contrast, substantial variability was observed for successive measurements on different molecules. This is expected since the orientation of the molecules and the precise location and pressure of the probe will vary from molecule to molecule.

A complementary measurement is the measurement of the average conductivity through many molecules. A significant problem was the creation of a top electrode over a layer of ferritin molecules adsorbed onto a gold surface. An evaporated metal layer would create electrical shorts to the underlying gold in gaps between ferritin molecules. Additionally the metal evaporation process would heat the molecules, possible denaturing the protein. To avoid these problems a 500 micron gold ball suspended from a gold wire was used to make a room temperature contact to a few thousand ferritin molecules. To form the ball, the end of a gold wire with a diameter about 0.1 millimeters was heated in a high temperature flame and cooled prior to bringing it into contact with the surface. Example balls are shown in Figure 27. Figure 28 shows the current-voltage data for apo and holoferritin measured with the gold ball contact. Both the contact force applied and the ferritin concentration on the surface were similar for the samples measured. The results show a significantly higher conductivity for holoferritin, consistent with the measurements made on single molecules.

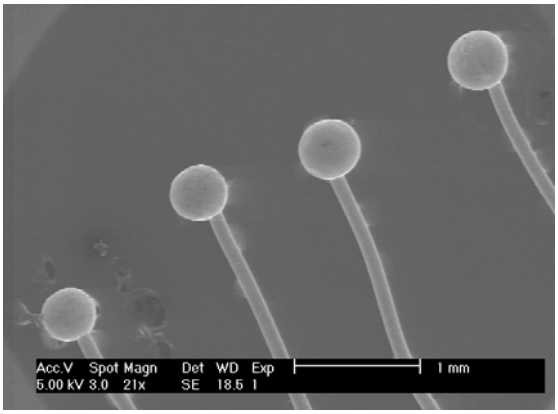

Figure 27. SEM image of four gold balls formed on the ends of gold wire with diameter 0.1 millimeters.

<u>Fabrication of Microelectronic Chip and Micropatterned Multi Electrodes.</u>

In order to proved metal electrode contact to the quantum logic dots, the Au metal lines were fabricated with e-beam lithography process as described below.

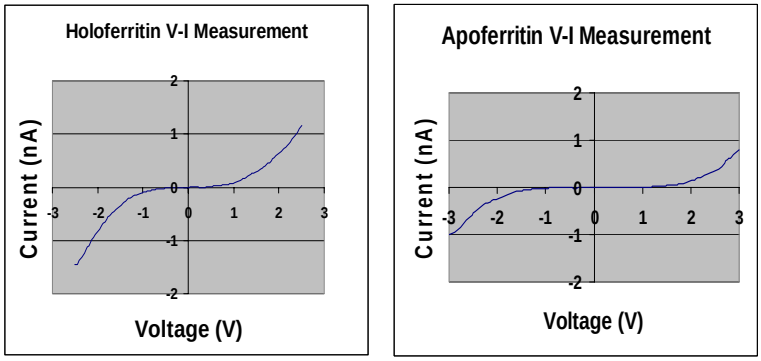

Figure 28. Current vs. voltage curves for holo(left) and apo(right) ferritin measured with a 500 micron diameter gold ball.

- E-Beam Lithography CAD file was created with a 1,024 x 1,024 pixels resolution bitmap image. The minimum feature size was 0.5μm.
- Thin gold film with a thickness of 200nm was sputter-deposited on glass. Post annealing of Au film was performed at 300°C in a vacuum for 4 hours.

- The electron resist, PMMA in anisol solution, was spin-coated and hard-baked at 150°C for one hour before the sample was introduced into SEM chamber. 20pA of electron beam current was used with the point dose of 1.7fC. The aerial dose was about 400μC/cm^2.
- The scanning position of electron beam and the beam exposure time were controlled by a computer to generate the desired pattern of bitmap CAD file. 2X2 virtual spots were written between bitmap pixels to fill in the space between e-beam diameters.
- After the e-beam lithography and the soft-bake, 3:1 IPA:MIBK developer was used to remove the e-beam exposed area.
- The exposed gold thin-film was removed with an iodine containing wet-etchant.
- After the etching, the remaining PMMA was removed in acetone.

The following figure shows the fabricated microelectrodes for (1) a simple junction and (2) a complex 5-way circuit. The minimum gap distance was about 1μm.

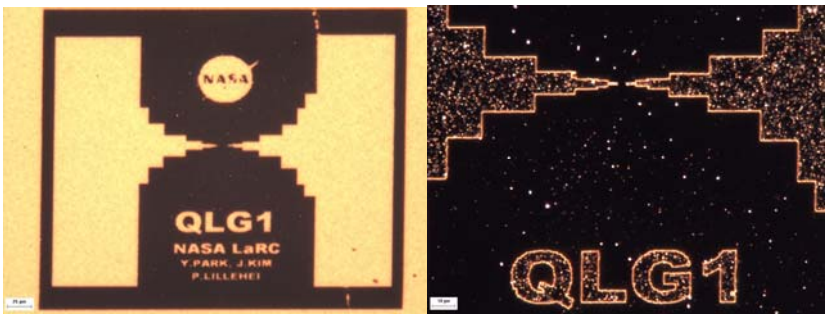

Figure 29. (Left) Optical microscope image of a simple junction electrode, (Right) Dark field zoomed image of the simple junction.

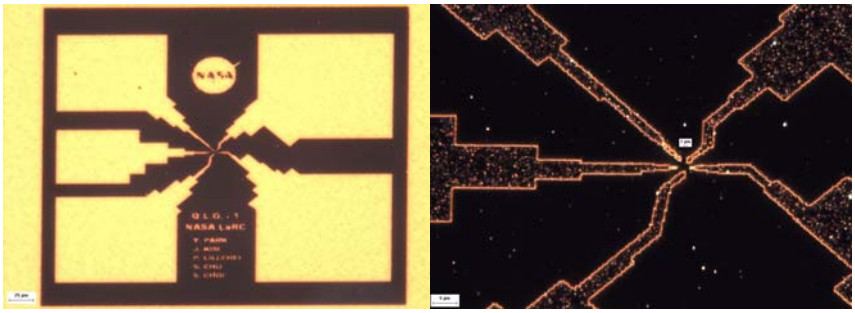

Figure 30. (Left) Optical microscopic image of 5-way circuit for Quantum Logic Gate, (Right) Dark field image of the junction area in 5-way circuit.

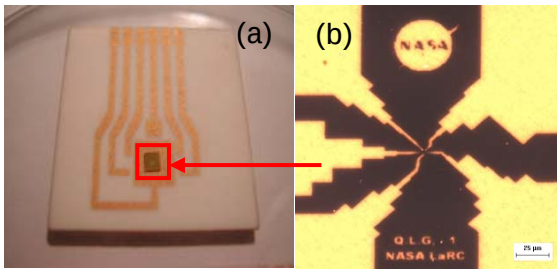

Figure 31. (a) Microelectronic chip fabrication for ferritin-based quantum logic gates test. (b) Micropatterned electrodes prepared by e-beam lithography. Scale bar is 25 μm.

REFERENCES:

[1] P. M. Harrison and P. Arosio, *Biochim. Biophys. Acta,* **161**, 1275 (1996).
[2] D. D. Awschalom, J. F. Smyth, G. Grinstein, D. P. DiVincenzo, and D. Loss, *Phys. Rev. Lett., **68***, 3092 (1992).
[3] S. Gider, D. D. Awschalom, T. Douglas, S. Mann, and M. Chaparala, *Science,* **268**, 77 (1995).
[4] J. Tejada, X. X. Zhang, E. del Barco, J. M. Hernandez, and E. M. Chudnovsky, *Phys. Rev. Lett., **79***, 1754 (1997).
[5] D. Loss and D. P. DiVincenzo, *Phys. Rev. A, **57***, 120 (1998).
[6] M. A. Nielsen and I. L. Chuang, *Quantum Computation and Quantum Information*, Cambridge University Press, Cambridge, UK (2000).
[7] J. Tejada, E. M. Chudnovsky, E. del Barco, J. M. Hernandez, and T. P. Spiller, *Nanotechnology, **12***, 181 (2001).
[8] E. del Baco, J. M. Hernandez, M. Sales, J. Tejada, H. Rakoto, J. M. Broto, and E. M. Chudnovsky, *Phys. Rev. B, **60***, 11898 (1999).
[9] A. Barenco, C. M. Bennett, R. Cleve, D. P. DiVincenzo, N. Margolus, P. Shor, T. Sleator, J. A. Smolin, and H. Weinfurter, *Phys. Rev. A, **52***, 3457 (1995).
[10] T. Ohshima, H. Z. Song, Y. Okada, K. Akahane, T. Miyazawa, and M. Kawabe, *Phys. Stat. Sol. C, **0***, 1364 (2003).
[11] T. Douglas and V. T. Stark, *Inorg. Chem., **39***, 1828 (2000).
[12] F. C. Meldrum, V. J. Wade, D. L. Nimmo, B. R. Heywood, and S. Mann, *Nature, **349***, 684 (1991).
[13] P. Mackle, J. M. Charnock, C. D. Garner, F. C. Meldrum, and S. Mann, *J. Am. Chem. Soc., **115***, 8471 (1993).
[14] F. C. Meldrum, T. Douglas, S. Levi, P. Arosio, and S. Mann, *J. Inorg. Biochem., **58***, 59 (1995).
[15] M. Okuda, K. Iwahori, I. Yamashita, and H. Yoshimura, *Biotech. Bioengineer., **84***, 187 (2003).
[16] K. K. W. Wong and S. Mann, *Adv. Mater., **8***, 928 (1996).
[17] F. C. Meldrum, B. R. Heywood, and S. Mann, *Science, **257***, 522 (1992).
[18] K. K. W. Wong, T. Douglas, S. Gider, D. D. Awschalom, and S. Mann, *Chem. Mater., **10***, 279 (1998).
[19] H. Z. Song, K. Akahane, S. Lan, H. Z. Xu, Y. Okada, and M. Kawabe, *Phys. Rev. B, **64***, 085303 (2001).
[20] H. Lee, J. A. Johnson, J. S. Speck, and P. M. Petroff, *J. Vac. Sci. Technol. B, **18***, 2193 (2000).
[21] M. Borgstrom, J. Johansson, L. Samuelson, and W. Seifert, *Appl. Phys. Lett., **78***, 1367 (2001).
[22] S. Kohmoto, H. Nakamura, T. Ishikawa, and K. Asakawa, *Appl. Phys. Lett., **75***, 3488 (1999).
[23] J. Tejada, *Polyhedron, **20***, 1751 (2001).
[24] I. Yamashita, *Thin Solid Films, **393***, 12, (2001).
[25] L. Jelinski, *Biologically Related Aspects*, in *Nanostructure Science and Technology: R&D Status and Trends in Nanoparticles, Nanostructured Materials, and Nanodevices*, Edited by R. W. Siegel, E. Hu, and M. C. Roco, WTEC Panel Report, National Science and Technology Council, (1999).
[26] M. Zborowski, C. B. Fuh, R. Green, N. J. Baldwin, S. Reddy, T. Douglas, S. Mann, and J. J. Chalmers, *Cytometry, **24***, 251 (1996).
[27] F. Torres, J. M. Hernandez, X. Bohigas, and J. Tejada, *Appl. Phys. Lett., **77***, 3248 (2000).
[28] M. Darder, K. Takada, F. Pariente, E. Lorenzo, and H. D. Abrũna, *Anal. Chem., **71***, 5530 (1999).
[29] R. Jue, J. M. Lambert, L. R. Pierce, and R. R. Traut, *Biochemistry, **17***, 5399 (1978).
[30] J. M. Lambert, R. Jue, and R. R. Traut, *Biochemistry, **17***, 5406 (1978).
[31] E. Pavlovic, A. P. Quist, U. Gelius, and S. Oscarsson, *J. Colloid. Interface Sci., **254***, 200 (2002).
[32] M. Hu, S. Noda, Y.Tsuji, T. Okubo, Y.Yamaguchi, and H. Komiyama, *J. Vac. Sci. Technol. A, **20***, 589 (2002).
[33] A. Treffry and P. M. Harrison, *Biochem. J.*, **171**, 313 (1978).
[34] G. Zhao, F. Bou-Abdallah, X. Yang, P. Arosio, and D. Chasteen, *Biochemistry*, **40**, 10832 (2001).
[35] B. Zhang, S.-H. Chu, S. H. Choi, J.-W. Kim, J. H. Harb, R. C. Davis, and G. D. Watt, *Inorg. Chem.,* Under revision (2004).
[36] B. Zhang, J. H. Harb, R. C. Davis, S.-H. Chu, S. H. Choi, J.-W. Kim, and G. D. Watt, *Inorg. Chem.,* Under revision (2004).